References

[1]Dyment, A., and Merlen, A., "Gun Firing Similarity for Aircraft Interference Problems," *Journal of Aircraft*, Vol. 18, No. 5, 1981, pp. 415, 416.

[2]Merlen, A., and Dyment, A., "Similarity and Asymptotic Analysis for Gun Firing Aerodynamics," *Journal of Fluid Mechanics*, Vol. 225, pp. 497–528.

Viscous Flow Past a Nacelle in Proximity to a Flat Plate

Kamran Fouladi*

Lockheed Engineering and Sciences Company, Inc., Hampton, Virginia 23666

Introduction

VARIOUS conceptual designs for a commercial supersonic transport have been developed in recent years. Most of these configurations have been designed using linearized and modified linearized potential theory methodologies[1–5] to define the vehicle shape and the aerodynamic characteristics. Other methods based on Whitham's modified linear theory[6–8] have been used in the design and analysis of low-boom configurations. The combination of these methods has proven to be useful in the preliminary design stage of low-boom, high-speed civil transport configurations.

In estimating the overall aerodynamic characteristics of a configuration with nacelles, the interference effects must be evaluated. The lift induced by nacelles on the wing lower surface adds to the equivalent body area distributions composed of volume and lift contributions. The equivalent body area rule defines Whitham's F-function, which in turn renders the far-field overpressure signatures of a supersonic aircraft. The computational technique described in Ref. 4 provides estimations of the loads imposed on a wing surface by nacelles mounted nearby. This numerical method, however, is impaired by its inability to account for certain nonlinear effects inherent in complicated flows. The qualitative analyses of wind-tunnel data for various aircraft models with nacelles have suggested that the interference pressures, calculated using the computer program of Ref. 4, might be underestimated in the extreme near field. Therefore, more accurate estimates of the extreme near-field conditions are required to improve the design of low-boom supersonic transport configurations.

The purpose of the present study is to perform Navier–Stokes calculations in order to provide pressure distributions and force data on a flat plate with a nacelle in close proximity. The pressure distributions obtained using Navier–Stokes equations are then compared with the pressure distributions obtained using the linear theory of Ref. 4. Incorporating the nacelle-induced lift on the wing into the design process of a low-boom transport configuration will be included in a follow-up study. The Navier–Stokes equations are solved by an implicit, approximately factored, finite volume, upwind algorithm.[9,10] Baysal et al.[9] have used this algorithm to compute a supersonic flow past an ogive-nose-cylinder at zero-deg angle of attack near a flat plate on a composite mesh of overlapped grids. Fouladi et al.[10–11] extended the algorithm to include the use of a hybrid domain decomposition method that takes advantage of strengths of various techniques such as multiblock structured grids, zonal grids, or overlapped grids. This Note presents the numerical investigations of viscous supersonic flows past a circular nacelle placed in close proximity to a flat plate. The interference flowfield between these two geometrically nonsimilar components is simulated for several freestream Mach numbers.

Received Dec. 12, 1994; revision received June 12, 1994; accepted for publication Feb. 22, 1995.

*Engineer, Aeronautics and Management Support Department, Langley Program Office.

Results and Discussion

In the present investigation, a circular nacelle is placed in close proximity to a flat plate. The nacelle is 36 ft long and its schematic is detailed in Fig 1. Inlet and exhaust diameters of the nacelle are 6.0 and 9 ft, respectively. The flat plate is 41.86 ft long and 14.44 ft wide, and it is located 5.5 ft from the nacelle centerline. The longitudinal center planes of the nacelle and the flat plate are aligned. Two multiblock-structured Cartesian grids represent the upper (105 × 29 × 25) and lower (105 × 29 × 37) sides of the flat plate, and they are both overlapped on the outer H—O grid (105 × 33 × 45) of the nacelle. The inner H—O grid (93 × 33 × 33) of the nacelle is matched with the outer grid of the nacelle along the nacelle wall. The total number of grid points for this composite grid is 445,992. Only half of the configuration is analyzed because the model is symmetric and at zero yaw angle. The computational time and run-time memory for the present computations on the Cray-2 at the NASA Langley Research Center are approximately 6 CPU hours and 17 MWords, respectively.

The boundary conditions are specified explicitly in this implicit scheme. The conventional viscous boundary conditions are imposed on all solid surfaces. The upstream boundaries are all specified. First-order extrapolations of the primitive variables are used along the downstream boundary. One-dimensional characteristic boundary conditions are imposed at the outer boundary of the nacelle and at top and spanwise outboard boundaries of the flat plate. Reflection boundary conditions are used on the plane of symmetry. Intergrid boundaries also exist between overlapped subdomains that do not coincide with the physical boundaries of the computational domain. The boundary conditions for the intergrid boundaries are given in detail in Ref. 9. Three different freestream Mach numbers M_∞ of 1.6, 2.0, and 2.3 are considered.

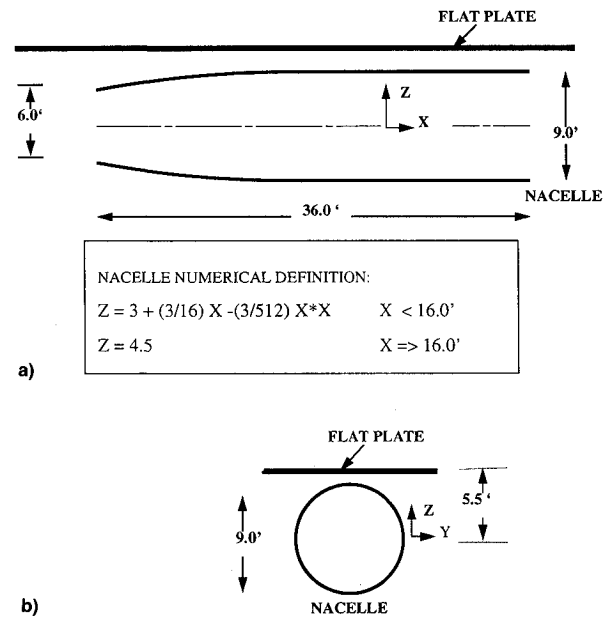

Fig. 1 Schematic of the nacelle in proximity to the flat plate: a) side and b) back view.

The approaching flows are assumed to be fully turbulent and at zero incidence. The freestream Reynolds number/ft is 2×10^6 and the freestream total temperature is 585°R.

Prior to the investigation of interference flow between the nacelle and the flat plate, supersonic flow past an isolated nacelle is simulated to establish a reference for the nacelle-flat plate case. The Mach number contours on the symmetry plane for the isolated nacelle are presented in Fig. 2. Flow inside the nacelle is accelerated to a higher Mach number than freestream due to the divergent section of the nacelle. The boundary layer becomes thicker aft of this acceleration, resulting in a smaller passage area, which in turn slows the supersonic flow. The flow is then accelerated as it exits the nacelle. The pressure signatures on the plane of symmetry at 5.5 ft from the nacelle centerline are shown in Fig. 3. The signatures predicted by the linear theory method of Ref. 4 are also shown in this figure for comparison. Similar initial overpressure peaks due to the lip shock are predicted by both methods at $M_\infty = 1.6$ (Fig. 3a). At higher Mach numbers, the linear theory underpredicts the initial overpressure peak (Figs. 3b and 3c).

The longitudinal pressure distributions of the nacelle-flat plate are presented in Fig. 4. Pressure distributions are shown on the nacelle and the inboard side of the flat plate from the Navier–Stokes computations. The pressure distribution on the inboard side of the flat plate using the linear method of Ref. 4 is also shown in Fig. 4. The mutual interference between the nacelle and the flat plate is clearly shown at $M_\infty = 2.3$ (Fig. 4c) as the shock from the lip, designated as location A, is impinged on the flat plate at location B and reflected to the nacelle at location C. The recompression wave is then reflected off the nacelle and back on the flat plate at location

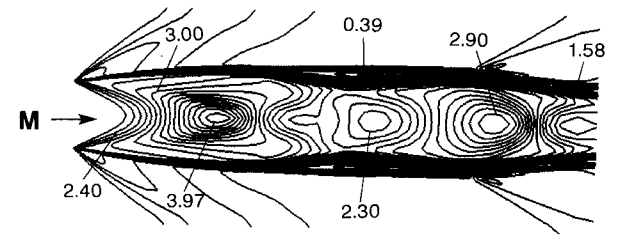

Fig. 2 Mach number contours on the symmetry plane of the isolated nacelle ($M_\infty = 2.3$).

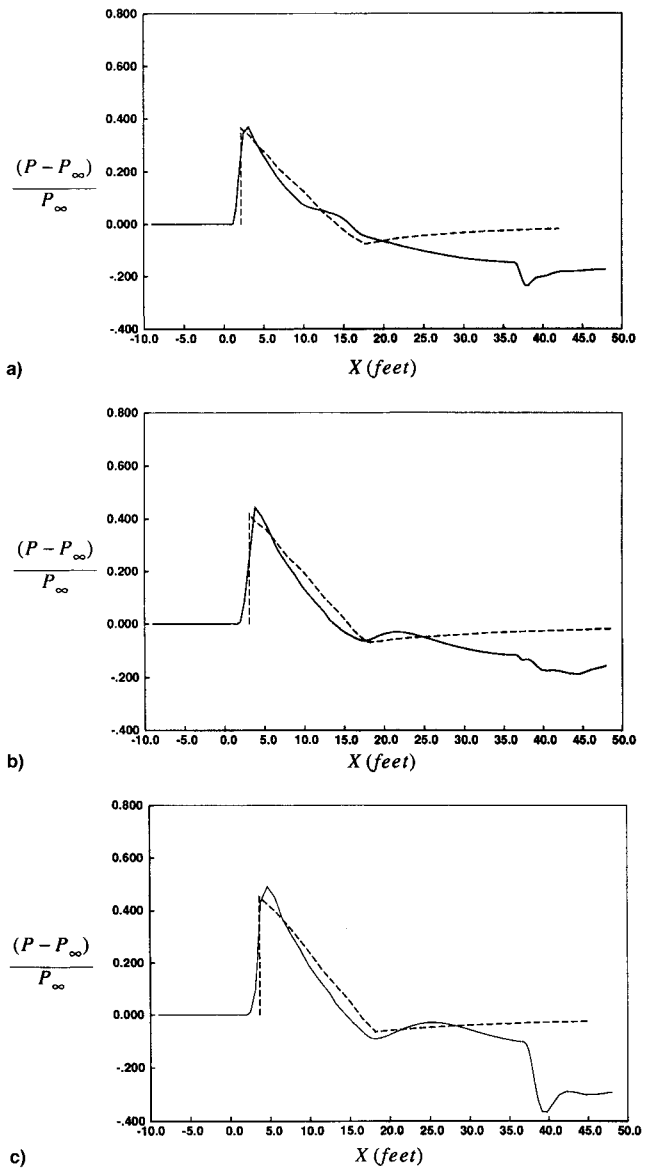

Fig. 3 Pressure signatures on the symmetry plane at 5.5 ft from the centerline of the isolated nacelle, M_∞ = a) 1.6, b) 2.0, and c) 2.3. —— = thin-layer Navier–Stokes and ---- = Ref. 4 (linear).

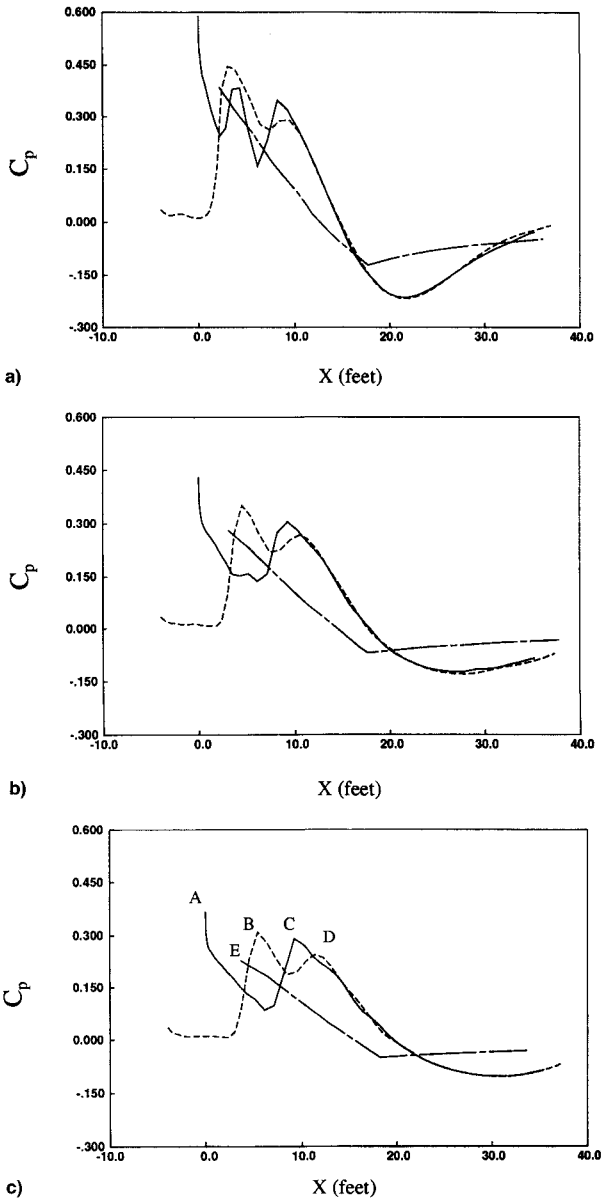

Fig. 4 Longitudinal surface pressure coefficient C_p on the inboard side of the nacelle and the flat plate, M_∞ = a) 1.6, b) 2.0, and c) 2.3. —— = nacelle (thin-layer Navier–Stokes), ---- = flat plate (thin-layer Navier–Stokes), and —·— = flat plate (Ref. 4, linear).

D. This is followed by overexpansion to pressures below the freestream. Strength of the initial shock is gradually attenuated due to its interaction with the boundary layers and the shape of the nacelle outer surface. Although the linear theory of Ref. 4 was adequate for predicting pressure signatures near an isolated nacelle, the pressure coefficient distribution on the flat plate using Ref. 4 illustrates the limitation of the linear theory for this configuration. An overexpansion to pressure below the freestream occurs downstream of location E where the nacelle lip shock impinges on the flat plate. Other shock reflections on the flat plate are not predicted. The interference pressures between the flat plate and the nacelle at $M_\infty = 1.6$ and 2.0 are similar to those observed at $M_\infty = 2.3$. However, the incident and reflected shock structure appears to be more complicated at $M_\infty = 1.6$ where some of the reflected shocks resemble normal shocks. The pressure distributions on the flat plate illustrate the lift induced on the flat plate by the nacelle. The normal force coefficient C_N on the flat plate is computed at each freestream Mach number. The values of C_N at $M_\infty = 1.6$, 2.0, and 2.3 are 0.026, 0.32, and 0.035, respectively. A reflexed wing can certainly reduce the negative pressure gradient on the inboard side and take advantage of the positive pressure gradient created due to the interference.

Concluding Remarks

Three-dimensional flows past an isolated nacelle and a nacelle in close proximity to a flat plate were computationally simulated. This was accomplished by solving the Navier–Stokes equations by an implicit, upwind-biased, finite volume method. The computational grids were generated using a hybrid domain decomposition technique. A multiblock grid was used for the isolated nacelle case. For the nacelle-flat plate case, both multiblock and grid overlapping techniques were utilized for easing the grid generation task for this complex configuration. The results indicated the significant limitations of the linearized method for accurately predicting the mutual interference between the components. The effects of Mach number on such flowfields were also investigated and are presented in the present study.

Acknowledgments

This work is supported under NASA Contract NAS1-19000. The Technical Monitor is C. M. Darden.

References

[1]Harris, R. V., Jr., "A Numerical Technique for Analysis of Wave Drag at Lifting Conditions," NASA TN D-3586, Oct. 1966.

[2]Carlson, H. W., and Miller, D. S., "Numerical Methods for the Design and Analysis of Wings at Supersonic Speeds," NASA TN D-7713, Dec. 1974.

[3]Carlson, H. W., and Mack, R. J., "Estimation of Wing Nonlinear Aerodynamic Characteristics at Supersonic Speeds," NASA TP-1718, Nov. 1980.

[4]Mack, R. J., "A Numerical Method for Evaluation and Utilization of Supersonic Nacelle-Wing Interference," NASA TN D-5057, March 1969.

[5]Middelton, W. D., and Lundry, J. L., "A Computational System for Aerodynamic Design and Analysis of Supersonic Aircraft. Part 1—General Description and Theoretical Development," NASA CR-2715, July 1976.

[6]Whitham, G., "The Flow Pattern of a Supersonic Projectile," *Communication on Pure and Applied Mathematics*, Vol. V, No. 3, 1952, pp. 301–348.

[7]Walkden, F., "The Shock Pattern of a Wing-Body Combination, Far from the Flight Path," *Aeronautical Quarterly*, Vol. IX, Pt. 2, 1985, pp. 164–194.

[8]Hayes, W., Haefeli, R., and Kulsrud, H., "Sonic-Boom Propagation in a Stratified Atmosphere, with a Computer Program," NASA CR-1299, April 1969.

[9]Baysal, O., Fouladi, K., and Lessard, V. R., "A Multigrid Method to Solve 3-D Viscous Equations on Overlapped and Embedded Grids," *AIAA Journal*, Vol. 29, No. 6, 1991, pp. 903–910.

[10]Fouladi, K., and Baysal, O., "Viscous Simulation Method for Unsteady Flows Past a Configuration with Nonsimilar Multicomponents," *Journal of Fluids Engineering*, Vol. 114, No. 1, 1992, pp. 161–169.

[11]Fouladi, K., Baysal, O., and Newman, J. C., "Hybrid Domain Decomposition for Configurations with Multiple Nonsimilar Components," SIAM 5th Conf. on Domain Decomposition Methods for Partial Differential Equations, Norfolk, VA, May 1991.

Wedge-Cone Waverider Configuration for Engine-Airframe Integration

Naruhisa Takashima* and Mark J. Lewis†
University of Maryland,
College Park, Maryland, 20742

Introduction

HYPERSONIC waveriders are promising shapes for the forebodies of engine-integrated hypersonic vehicles. These configurations can form the basis of airframes with very high lift-to-drag ratios (L/D). Furthermore, because they are designed with an inverse methodology, the flowfield is first selected, then the appropriate generating shape is determined; they lend themselves especially well to inlet optimization, as was shown by O'Neill and Lewis.[1] The resulting shapes provide relatively uniform inlet conditions, corresponding to the flow conditions of the original generating flow. O'Neill and Lewis integrated engines with a waverider forebody that were generated with a conical flowfield; a trailing-edge shape that defines the inlet curve was traced upstream from the inlet plane to carve the lower surface of the waverider. The shape was then optimized for maximum L/D by changing the shape of the trailing-edge curve and the shock angle. The center portion of the trailing-edge curve was fixed as an elliptical curve so that the difference in the normal distance between the shock and the surface in the spanwise direction could be minimized. This was done to allow the use of identical engine modules. Ideally, a circular arc instead of an elliptical curve should be used, however, this was shown to produce a waverider shape with potentially excessive aerodynamic heating in the nose and poor volumetric efficiency. By using an elliptical curve, the inlet flowfield will always have some nonuniformities. Also, because the generating flowfield is axisymmetric, there is a radially varying sidewash angle in the spanwise direction. The influence of the variation can be minimized by using multiple engine modules; however, each module will still experience flow nonuniformity in the radial direction.

Since these waverider inlet flow nonuniformities are a direct result of the conical nature of the design flowfield, it is of interest to examine other generating flowfields, particularly nonaxisymmetric shapes, for their ability to produce more uniform inlet properties. This work will focus on inlets derived from the flowfield associated with a hybrid wedge-cone combination.

Received Dec. 23, 1992; revision received May 3, 1994; accepted for publication Feb. 21, 1995.

*Graduate Research Assistant, Department of Aerospace Engineering. Student Member AIAA.

†Associate Professor, Department of Aerospace Engineering. Senior Member AIAA.